Letter

Diffusion as a possible mechanism controlling the production of superheavy nuclei in cold fusion reactions

T. Cap and M. Kowal*
National Centre for Nuclear Research, Pasteura 7, 02-093 Warsaw, Poland

K. Siwek-Wilczyńska
Faculty of Physics, Warsaw University, Pasteura 5, 02-093 Warsaw, Poland

(Received 16 February 2022; accepted 2 May 2022; published 16 May 2022)

The fusion probability for the production of superheavy nuclei in cold fusion reactions was investigated and compared with recent experimental results for ^{48}Ca, ^{50}Ti, and ^{54}Cr incident on a ^{208}Pb target. Calculations were performed within the fusion-by-diffusion model (FbD) using the new nuclear data tables by Jachimowicz *et al.* [At. Data Nucl. Data Tables **138**, 101393 (2021)]. It is shown that the experimental data could be well explained within the framework of the FbD model. The saturation of the fusion probability at bombarding energies above the interaction barrier is reproduced. It emerges naturally from the physical effect of the suppression of contributions of higher partial waves in fusion reactions. The role of the difference in values of the rotational energies in the fusion saddle point and contact (sticking) configuration of the projectile-target system is discussed.

DOI: 10.1103/PhysRevC.105.L051601

I. INTRODUCTION

Superheavy elements with atomic numbers $104 \leqslant Z \leqslant 113$ were discovered in cold fusion reactions in which closed-shell ^{208}Pb or ^{209}Bi target nuclei were bombarded with projectiles ranging from Ti to Zn [1,2].

The production cross section for superheavy nuclei (SHN) can be considered as the product of three factors: the cross section for the projectile to overcome the entrance channel barrier (capture cross section), the probability that the resulting system fuses and reaches the compound nucleus configuration, and the probability that the excited compound nucleus survives fission during deexcitation.

The optimal conditions to produce a given superheavy nucleus result from various factors. The increase in the symmetry between reaction partners requires higher bombarding energies to overcome the entrance channel barrier and enhances the contribution of fast nonequilibrium deep-inelastic (DIC) and quasifission (QF) processes preventing fusion. The fusion probability rapidly drops when the product of projectile and target nuclei atomic numbers $Z_1 \times Z_2 \geqslant 1600$ [3]. Therefore, the compound nucleus formation cross section represents only part of the capture cross section.

In cold fusion reactions, merging the strongly bound target and projectile nuclei leads to a weakly bound compound nucleus. Typically, SHN have higher thresholds for neutron emission [4] than the heights of the fission barrier [5], making fission the dominant deexcitation process. At each step of the deexcitation cascade, neutron evaporation competes with fission, which additionally reduces the final evaporation residue cross section.

The cross sections for the production of nuclei with $Z \geqslant 102$ in cold fusion reactions drop approximately seven orders of magnitude as the projectile atomic number changes from 20 (Ca) to 30 (Zn). The question of what the mechanism is that prevents the synthesis of SHN is still under discussion. A low survival probability is not enough to explain the extremely low production cross sections. One way of thinking about the additional hindrance mechanism is the concept of an internal barrier holding back (counteracting) the fusion process. Overcoming this barrier by a diffusion process and thermal fluctuations could help to reach the state of a compound nucleus.

Recently, the probability of compound nucleus formation P_{CN}, at energies around and above the interaction barrier B_0 was measured for ^{48}Ca, ^{50}Ti, and ^{54}Cr projectiles incident on a ^{208}Pb target [6]. By comparing the experimental data with the semiempirical expression based on the diffusion approach proposed by Zagrebaev and Greiner in Ref. [7], the authors of Ref. [6] concluded that "the energy dependence of P_{CN} indicates that cold fusion reactions (involving ^{208}Pb) are not driven by a diffusion process." This Letter aims to investigate the fusion probabilities for these reactions using the diffusion approach. Calculations are performed within the l-dependent fusion-by-diffusion model (FbD) [8] using the new nuclear data tables for SHN by Jachimowicz *et al.* [4] as input.

II. FUSION-BY-DIFFUSION MODEL

The fusion-by-diffusion model in its first form was a simple tool to calculate cross sections and optimum bombarding

*michal.kowal@ncbj.gov.pl

energies for a class of $1n$ cold fusion reactions [9,10]. A significant development of this model was the incorporation of the angular-momentum dependence, that is, the contributions from successive partial waves to the reaction cross section [8].

Due to the different timescales of the particular reaction stages, the partial evaporation residue cross section, $\sigma_{\rm ER}(l)$, can be factorized as the product of the partial capture cross section $\sigma_{\rm cap}(l) = \pi\lambda\!\!\!^{-2}(2l+1)T(l)$, the fusion probability $P_{\rm fus}(l)$, and the survival probability $P_{\rm surv}(l)$. Thus, the total evaporation residue cross section for the production of a given superheavy nucleus in its ground state is

$$\sigma_{\rm ER} = \pi\lambda\!\!\!^{-2}\sum_{l=0}^{\infty}(2l+1)T(l)P_{\rm fus}(l)P_{\rm surv}(l), \tag{1}$$

where $\lambda\!\!\!^{-}$ is the wavelength, and $\lambda\!\!\!^{-2} = \frac{\hbar^2}{2\mu E_{\rm c.m.}}$. Here μ is the reduced mass of the colliding system, and $E_{\rm c.m.}$ is the center-of-mass energy at which the reaction takes place.

The method of calculating the capture cross section is described in the next section. The fusion probability is described in detail in Sec. II B.

The last factor in Eq. (1), the survival probability, is calculated by applying classical transition-state theory using nuclear data from Ref. [4]. Details regarding this reaction stage for $1n$ cold fusion reactions can be found in Ref. [8].

A. Capture cross section

The capture transmission coefficients $T(l)$ in Eq. (1) are calculated in a simple sharp cutoff approximation, where the upper limit $l_{\rm max}$ of full transmission, $T(l) = 1$, is determined from the empirical systematics of the capture cross sections for heavy nuclear systems.

Following the experimental results, the entrance channel barrier is not described by a single value but by a distribution that can be approximated by a Gaussian shape described by two parameters, the mean barrier B_0 and the distribution width ω [11]. Folding the Gaussian barrier distribution with the classical expression for the fusion cross section leads to the formula for the capture cross section

$$\sigma_{\rm cap} = \pi R^2\frac{\omega}{E_{\rm c.m.}\sqrt{2\pi}}\{X\sqrt{\pi}[1+{\rm erf}(X)] + \exp(-X^2)\} = \pi\lambda\!\!\!^{-2}(l_{\rm max}+1)^2, \tag{2}$$

where $X = \frac{E_{\rm c.m.}-B_0}{\omega\sqrt{2}}$. The empirical systematics of B_0, ω, and the normalization factor R were obtained from analyzing precisely measured fusion or capture excitation functions for about 50 heavy nuclear systems for which the fusion probability is equal or close to unity [11]. In this paper we use the parametrizations of B_0, w, and R of Ref. [8].

B. Fusion probability

The second factor in Eq. (1), $P_{\rm fus}(l)$, is the probability that, after reaching the capture configuration, the colliding system will eventually overcome the fusion saddle point and merge, avoiding reseparation. It is assumed in the FbD model that, after sticking, a neck between the target and projectile nuclei rapidly grows at an approximately fixed mass asymmetry and elongation [9,10] bringing the system to the "injection point" somewhere along the bottom of the entrance channel asymmetric fission valley. The shape parametrization used to describe the interacting system is that of two spheres joined smoothly by a third quadratic surface. The elongation of the system is defined as $L = 2(R_1+R_2)+s$, where R_1 and R_2 are the radii of the colliding nuclei and s is the distance between two spheres.

Let us denote the elongation of the system at the injection point by $L_{\rm inj}$. The localization of this point with respect to the macroscopic conditional saddle (at the elongation $L_{\rm sd}$) is crucial for the fusion process. If $L_{\rm inj} > L_{\rm sd}$ the system is still "outside" the barrier separating the injection point from the compound nucleus configuration and must climb uphill to overcome the saddle. If $L_{\rm inj} < L_{\rm sd}$ the injection point configuration is more compact than the saddle configuration, and the system is already "inside" (behind the barrier). In this case, the barrier guards the system against reseparation by reducing the outgoing flux of particles.

In the diffusion approach, transition over the barrier happens by thermal fluctuations in the shape degrees of freedom. In case of strong friction, the Langevin equation can be replaced by its overdamped version, i.e., the Smoluchowski diffusion equation, see e.g., Refs. [12,13]. The fusion probability, $P_{\rm fus}(l)$, may be derived by solving this equation [9]. With the assumption that the internal barrier has height $H(l)$ and is of inverted parabola form one gets

$$P_{\rm fus}(l) = \frac{1}{2}\begin{cases}1+{\rm erf}\sqrt{H(l)/T}, & L_{\rm inj} < L_{\rm sd}\\ 1-{\rm erf}\sqrt{H(l)/T}, & L_{\rm inj} \geqslant L_{\rm sd},\end{cases} \tag{3}$$

where T is the average temperature of the fusing system (see Ref. [8] for details).

The energy threshold in Eq. (3) is taken as the difference between the energy of the fusion saddle point $E_{\rm sd}$ and the energy of the combined system at the injection point $E_{\rm inj}$, corrected by the appropriate rotational energies,

$$H(l) = \left[E_{\rm sd}+E_{\rm sd}^{\rm rot}(l)\right] - \left[E_{\rm inj}+E_{\rm inj}^{\rm rot}(l)\right]. \tag{4}$$

The energies $E_{\rm sd}$ and $E_{\rm inj}$ are calculated by using algebraic expressions (see Ref. [8]) that approximate the potential-energy maps obtained by Błocki and Świątecki [14]. The maps incorporate the most significant collective variables describing the fusion process, such as mass asymmetry, neck variable, and the system's elongation using the shape parametrization of two spheres joined smoothly by a third quadratic surface. The corresponding values of the rotational energies at the injection point $E_{\rm inj}^{\rm rot}(l)$ and the saddle point $E_{\rm sd}^{\rm rot}(l)$ are calculated assuming the rigid-body moments of inertia for the respective shapes [8].

The distance between the nuclear surfaces of two colliding nuclei at the injection point, $s_{\rm inj}$, is the only adjustable parameter of the model. It defines the onset of the diffusion process, thus, the moment when the available kinetic energy that remains after passing the entrance barrier is already transformed into internal degrees of freedom in the overdamped regime.

In this paper, we redefine the systematics of this crucial parameter based on a new set of ground-state and saddle-point properties of SHN [4]. The new parametrization of the

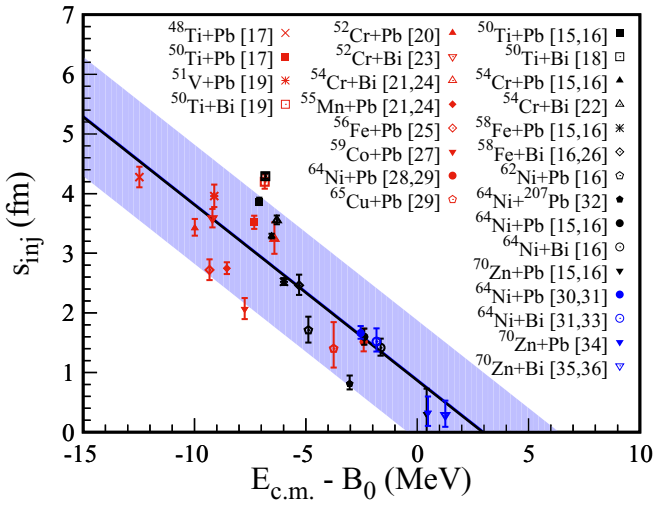

FIG. 1. The injection point systematics obtained for the set of $1n$ cold fusion reactions [15–36] using new nuclear data tables [4]. If not indicated otherwise, the targets were ^{208}Pb or ^{209}Bi. The color of the points indicates the laboratory where the reaction was studied: LBNL (red), GSI (black), RIKEN (blue). See text for details.

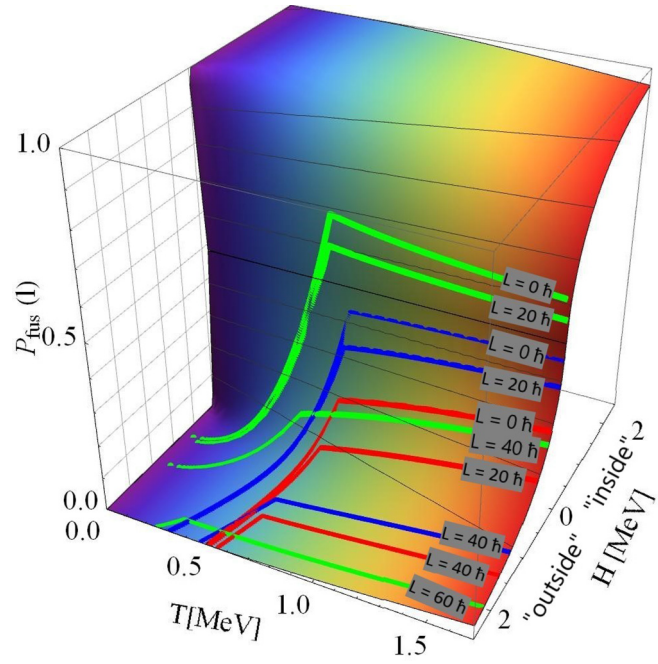

FIG. 2. Fusion probability $P_{fus}(l)$ as a function of temperature T and the barrier height opposing fusion $H(l)$. Lines correspond to selected angular momenta $l = 0\hbar$, $20\hbar$, $40\hbar$, and $60\hbar$. Calculations for ^{48}Ca + ^{208}Pb (green lines), ^{50}Ti + ^{208}Pb (blue lines), and ^{54}Cr + ^{208}Pb (red lines) fusion reactions. The color of the surface marks the temperature gradient of the synthesized system. The labels "outside" and "inside" refer to the injection point position relative to the saddle [see Eq. (3) and its discussion].

"injection point distance" is shown in Fig. 1 as a function of the excess of the center-of-mass energy $E_{c.m.}$ over the mean barrier B_0. Each point represents the value of the s_{inj} distance obtained by fitting Eq. (1) to the maxima of the experimentally measured $1n$ evaporation residue cross sections for 27 cold fusion reactions (see Ref. [8] for fitting protocol details).

It can be seen from Fig. 1 that, for energies up to a few MeV above B_0, the s_{inj} distance can be well approximated by a straight line given by

$$s_{inj} = 0.878\,\text{fm} - 0.294(E_{c.m.} - B_0)\ \text{fm/MeV}. \qquad (5)$$

A similar linear trend of s_{inj} as a function of $E_{c.m.} - B_0$ was reported in Ref. [12] by solving Langevin-type equations.

The shaded area in Fig. 1 represents an error corridor of ± 1 fm, which allows the uncertainty of the calculated fusion probabilities to be determined. The parametrization given by Eq. (5) should be used for interpolation rather than extrapolation far beyond the explored range of $E_{c.m.} - B_0$ values, especially if the extrapolation leads below the physically acceptable limit of the touching configuration ($s_{inj} \approx 0$). Negative values of this parameter would correspond to a large overlap of the density distributions at the sticking stage, an effect that is impossible in nuclear collisions at low bombarding energies. Therefore, in collisions at energies higher than a few MeV above B_0, we assume $s_{inj} = 0$ (allowing a deviation in the range of 1 fm).

III. RESULTS AND DISCUSSION

The FbD model with the new injection point distance parametrization and input data taken from Ref. [4] was used to analyze fusion probabilities for ^{48}Ca, ^{50}Ti, and ^{54}Cr reactions incident on a ^{208}Pb target.

The fusion probability given by Eq. (3) depends on the ratio of the height of the barrier opposing fusion $H(l)$ and the average temperature T of the system during the merging process. The fusion probabilities, $P_{fus}(l)$, for ^{48}Ca + ^{208}Pb (green lines), ^{50}Ti + ^{208}Pb (blue lines), and ^{54}Cr + ^{208}Pb (red lines) reactions as a functions of $H(l)$ and T are shown in Fig. 2 for a few selected l values.

At low energies the elongation of the system at the injection point is much larger than the elongation corresponding to the position of the conditional asymmetric (along the entrance channel fission valley) saddle. The symmetric saddle is even much more compact.

Let us start the discussion by analyzing the $l = 0$ case in which the height of the barrier is simply the difference between the asymmetric conditional saddle-point energy and the energy of the combined system of the projectile and target nuclei separated by the distance s_{inj} [see Eq. (4)]. As the available energy increases, the injection point distance decreases (see Fig. 1), leading to a lowering of the barrier height, and thus to the rapid growth of the fusion probability (see Fig. 2). When the separation distance reaches zero at the energy corresponding to $T \approx 0.6$–0.8 MeV, further energy increase does not change the height of the barrier (s_{inj} remains equal to zero) but heats the system up and thus affects the fusion probability. For the ^{48}Ca + ^{208}Pb reaction, the touching configuration is behind the asymmetric saddle point (as seen from the entrance channel perspective; inside regime in Fig. 2). In this case, the rising temperature increases the flux of particles escaping through the asymmetric saddle point and thus slightly reduces

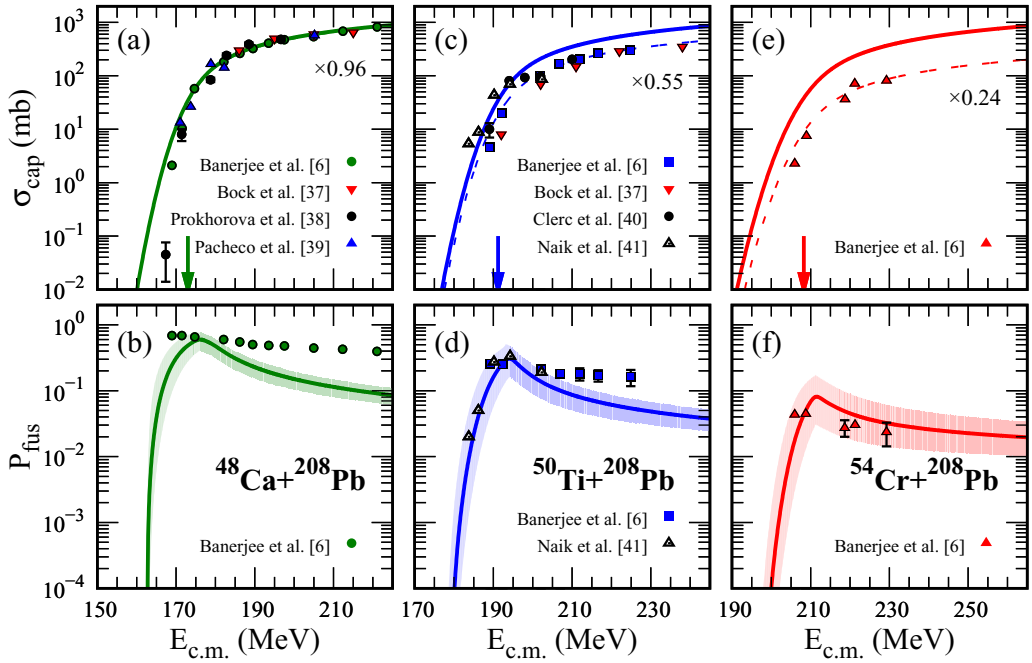

FIG. 3. Capture cross section σ_{cap} (top panels) and averaged fusion probability P_{fus} (bottom panels) for the reactions (a), (b) $^{48}Ca + ^{208}Pb$, (c), (d) $^{50}Ti + ^{208}Pb$, (e), (f) $^{54}Cr + ^{208}Pb$. Solid lines show the FbD model calculations of σ_{cap} and P_{fus}. Dashed lines in the top panels show calculated σ_{cap} scaled by the indicated suppression factors. The arrows indicate the value of the mean entrance channel barrier B_0 for each reaction. The error corridors resulting from the s_{inj} systematics uncertainty are shown as shaded areas in the bottom panels. Points represent relevant experimental data taken from Refs. [6,37–41]. If not shown, error bars are smaller than the symbol sizes.

the fusion probability [see $L_{inj} < L_{sd}$ case in Eq. (3)]. For ^{50}Ti and ^{54}Cr projectiles, the touching configuration is still outside the barrier and the fusion probability slowly increases with the increase of the incident energy [$L_{inj} \geqslant L_{sd}$ case in Eq. (3)].

The inclusion of the higher partial waves affects the entire potential-energy surface topology and influences the competition between the existing symmetric and asymmetric saddle points. In particular, the symmetric saddle, being more compact and having a lower moment of inertia, is more sensitive to the increase of the angular momenta. Above a certain l value, the symmetric saddle begins to dominate and becomes the main point to overcome in the fusion process for all studied systems. In this case, $P_{fus}(l)$ is calculated with respect to the symmetric saddle. In the corresponding $L_{inj} > L_{sd}$ regime of Eq. (3), the contribution of higher partial waves to the fusion cross section is gradually suppressed. The basic mechanism leading to the formation of the compound nucleus is based on two opposite effects. On the one hand the higher the excitation energy, the more partial waves contribute to the process. For a given excitation energy, the formula σ_{cap} defines a series of partial waves that are included in calculations (defining at the same time the maximum angular momentum above which the reaction does not take place). On the other hand the increase of angular momentum causes a corresponding increase in rotational energy (larger as the system becomes more compact due to smaller values of the moment of inertia). This leads to a higher centrifugal barrier and consequently diminishing $P_{fus}(l)$ values. The systematic decrease of the $P_{fus}(l)$ with the increase of the l value observed in Fig. 2 for all three reactions might also be viewed as a manifestation of the well-known effect of the limiting angular momentum to fusion.

As one can see in Fig. 2, the dominant contribution to the analyzed cold fusion reactions comes from near-central collisions. The more peripheral collisions are less favorable and lead to the reseparation of the system at the beginning of the nuclear reaction, rather than merging of target and projectile nuclei.

To study the effective fusion probability for a given reaction, one can define the quantity

$$P_{fus} = \frac{1}{(l_{max}+1)^2} \sum_{l=0}^{l_{max}} (2l+1) P_{fus}(l), \tag{6}$$

which is the fusion probability "averaged" over all angular momenta contributing to the fusion cross section.

In Fig. 3 we present a comparison of the FbD model predictions with the experimental data. The top panels show the capture cross sections for each of the reactions (i.e., cross sections for overcoming the entrance channel barrier) calculated using Eq. (2). Model calculations are compared with experimental data taken from Refs. [6,37–41]. The arrows in Figs. 3(a), 3(c), and 3(e) indicate the values of the mean entrance channel barriers B_0, calculated using the empirical parametrization [8], 173.0, 191.2, and 208.3 MeV for ^{48}Ca, ^{50}Ti, and ^{54}Cr, respectively.

The experimentally measured fission-like cross sections shown in the top panels of Fig. 3 lie below our calculations (solid lines). The deviation increases with increasing projectile atomic number. As proposed in Ref. [6],

we estimated scaling factors S for our calculations to reproduce the experimental results in the energy range above B_0. These factors are 0.96 for ^{48}Ca + ^{208}Pb, 0.55 for ^{50}Ti + ^{208}Pb, and 0.24 for ^{54}Cr + ^{208}Pb (in Ref. [6] the respective factors are 0.75, 0.48, and 0.22). Scaled capture cross sections are shown as dashed lines in Fig. 3.

Our scaling factors are in reasonable agreement with the results presented in Ref. [6], where they were estimated as a deviation from the CCFULL model based on the coupled channels formalism [42]. The capture cross section suppression might be associated with mass-asymmetric fast nonequilibrium processes, such as QF or DIC, appearing just after the interacting system passes the entrance channel barrier. It should be emphasized that both in this work and in Ref. [6], the scaling factors obtained are model-dependent.

Calculated averaged fusion probabilities [see Eq. (6)] for ^{48}Ca, ^{50}Ti, and ^{54}Cr reactions on a ^{208}Pb target are shown in the lower panels of Fig. 3. Full points in Figs. 3(b), 3(d), and 3(f) represent upper limits on the compound nucleus formation probabilities $P_{\rm sym}$ taken from Ref. [6]. $P_{\rm sym}$ is derived as the ratio of the measured symmetric-peaked fission cross section $\sigma_{\rm sym}$ to the capture cross section taken as the measured total fission-like cross section $\sigma_{\rm fis}$ divided by the appropriate scaling factor S [$P_{\rm sym} = \frac{\sigma_{\rm sym}}{\sigma_{\rm fis}/S}$, see Eq. (1) in the Supplemental Material of Ref. [6]].

For the ^{50}Ti + ^{208}Pb reaction additional experimental points [open triangles in Fig. 3(d)] taken from Ref. [41] are shown. These data were derived by measuring the angular distribution of mass-symmetric fission.

The calculated averaged fusion probabilities [Eq. (6), solid lines in Figs. 3(b), 3(d), and 3(f)] are in the low-energy region in good agreement with the experimental data for all reactions studied. A rapid decrease of the fusion probability in the energy region below B_0 reported in Ref. [41] for the ^{50}Ti + ^{208}Pb reaction is reproduced in our calculations [see Fig. 3(d)]. Unfortunately, the data for other reactions are limited in this energy region.

For each reaction, the maximum value of $P_{\rm fus}$ is reached for an energy a few MeV above B_0 (when $s_{\rm inj} \approx 0$). The steady decrease of $P_{\rm fus}$ with increasing energy is then due to the inclusion of higher partial waves.

Finally, in Fig. 4, we show the FbD model calculations of compound nucleus formation cross sections, defined as

$$\sigma_{\rm fus} = \pi\lambda\!\!\!^{-2} \sum_{l=0}^{l_{\rm max}} (2l+1) T(l) P_{\rm fus}(l) = \sigma_{\rm cap} P_{\rm fus}. \qquad (7)$$

The model calculations (solid lines) are compared with the symmetric-peaked fission cross sections measured in Ref. [6] but not given in that paper. Therefore, we deduced $\sigma_{\rm sym}$ values from the data using the relation $\sigma_{\rm sym} = P_{\rm sym}(\sigma_{\rm fis}/S)$ (see Fig. 4 in Ref. [6] and Fig. 5 in the corresponding Supplemental Material). Although the comparison of $\sigma_{\rm sym}$ with $\sigma_{\rm fus}$ is not entirely unequivocal, it seems adequate. One can see a very good agreement of the calculated and experimental cross sections up to the center-of-mass energy a few MeV above B_0. For higher energies, the trend of the excitation functions for two reactions ^{48}Ca + ^{208}Pb and ^{50}Ti + ^{208}Pb are different. Model calculations show a decrease while the experimental data show an increase. Experimental data shown in Fig. 4 may be overestimated due to incomplete subtraction of the QF background. On the other hand, the model may underestimate the fusion cross sections at higher excitation energies. This might be due to inaccurate estimation of the temperature and thus overestimation of the fusion hindrance.

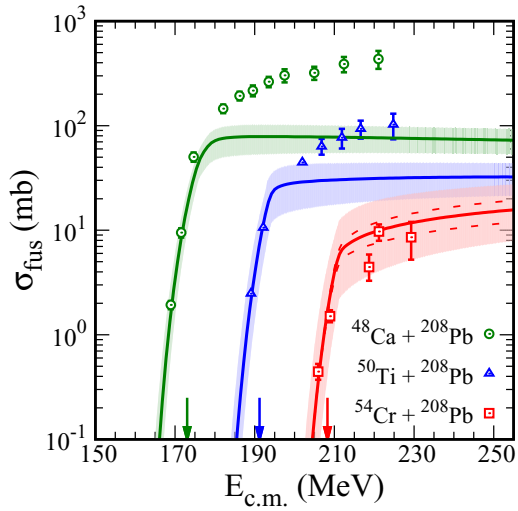

FIG. 4. Calculated compound nucleus formation cross sections $\sigma_{\rm fus}$ for ^{48}Ca + ^{208}Pb, ^{50}Ti + ^{208}Pb, and ^{54}Cr + ^{208}Pb fusion reactions. Points are derived from the experimental data presented in Ref. [6]. Dashed lines show calculations for two extreme orientations of spherical target and ^{54}Cr projectile in the entrance channel. The arrows indicate the value of the mean entrance channel barrier B_0 for each reaction. See text for details.

Some additional subtle effects related to the deformation of the ^{54}Cr projectile might be expected. However, as we have checked (by analyzing collisions of the spherical target with two extreme orientations of deformed projectiles; dashed lines in Fig. 4), the results for extreme orientations in the entrance channel are within the error corridor resulting from the systematics of $s_{\rm inj}$.

IV. CONCLUSIONS

The presented results show that the compound nucleus formation cross sections and related fusion probabilities for ^{48}Ca, ^{50}Ti, and ^{54}Cr incident on a ^{208}Pb target could be quite well reproduced within the framework of the FbD model, using the diffusion approach. In the energy range below B_0, the fusion probability growth comes from the reduction in the height of the internal barrier opposing fusion with increasing bombarding energy. The fusion probability saturation above B_0 results from suppression of the contributions from higher partial waves. The difference between rotational energies in the fusion saddle and the contact (sticking) configuration at the beginning of the fusion process plays a major role in compound nucleus formation at energies above B_0.

ACKNOWLEDGMENT

M.K. was co-financed by the International Research Project COPIGAL.

[1] S. Hofmann, Radiochim. Acta **99**, 405 (2011).
[2] K. Morita, K. Morimoto, D. Kaji, H. Habaa, and H. Kudo, Prog. Nucl. Sci. Technol. **5**, 8 (2018).
[3] K. H. Schmidt and W. Morawek, Rep. Prog. Phys. **54**, 949 (1991).
[4] P. Jachimowicz, M. Kowal, and J. Skalski, At. Data Nucl. Data Tables **138**, 101393 (2021).
[5] P. Jachimowicz, M. Kowal, and J. Skalski, Phys. Rev. C **95**, 014303 (2017).
[6] K. Banerjee, D. J. Hinde, M. Dasgupta, E. C. Simpson, D. Y. Jeung, C. Simenel, B. M. A. Swinton-Bland, E. Williams, I. P. Carter, K. J. Cook, H. M. David, C. E. Dullmann, J. Khuyagbaatar, B. Kindler, B. Lommel, E. Prasad, C. Sengupta, J. F. Smith, K. Vo-Phuoc, J. Walshe, and A. Yakushev, Phys. Rev. Lett. **122**, 232503 (2019).
[7] V. Zagrebaev and W. Greiner, Phys. Rev. C **78**, 034610 (2008).
[8] T. Cap, K. Siwek-Wilczyńska, and J. Wilczyński, Phys. Rev. C **83**, 054602 (2011).
[9] W. J. Świątecki, K. Siwek-Wilczyńska, and J. Wilczyński, Acta Phys. Pol. B **34**, 2049 (2003).
[10] W. J. Swiatecki, K. Siwek-Wilczynska, and J. Wilczynski, Phys. Rev. C **71**, 014602 (2005).
[11] K. Siwek-Wilczyńska and J. Wilczyński, Phys. Rev. C **69**, 024611 (2004).
[12] D. Boilley, Y. Abe, B. Cauchois, and C. Shen, J. Phys. G **46**, 115102 (2019).
[13] Y. Abe, D. Boilley, Q. Hourdillé, and C. Shen, Prog. Theor. Exp. Phys. **2021**, 021D01 (2021).
[14] J. Blocki and W. J. Swiatecki, Nuclear-deformation energies according to a liquid-drop model with a sharp surface, Technical Report No. LBL-12811 (Lawrence Berkeley Laboratory, USA, 1982), https://www.osti.gov/biblio/6632591.
[15] S. Hofmann, F. Heßberger, D. Ackermann, S. Antalic, P. Cagarda, B. Kindler, P. Kuusiniemi, M. Leino, B. Lommel, O. Malyshev *et al.*, Nucl. Phys. A **734**, 93 (2004).
[16] S. Hofmann, Rep. Prog. Phys. **61**, 639 (1998).
[17] I. Dragojević, K. E. Gregorich, C. E. Düllmann, M. A. Garcia, J. M. Gates, S. L. Nelson, L. Stavsetra, R. Sudowe, and H. Nitsche, Phys. Rev. C **78**, 024605 (2008).
[18] F. Hessberger, S. Hofmann, D. Ackermann, V. Ninov, M. Leino, G. Munzenberg, S. Saro, A. Lavrentev, A. Popeko, A. Yeremin *et al.*, Eur. Phys. J. A **12**, 57 (2001).
[19] J. M. Gates, S. L. Nelson, K. E. Gregorich, I. Dragojevic, C. E. Dullmann, P. A. Ellison, C. M. Folden, M. A. Garcia, L. Stavsetra, R. Sudowe, D. C. Hoffman, and H. Nitsche, Phys. Rev. C **78**, 034604 (2008).
[20] C. M. Folden III, I. Dragojević, C. E. Düllmann, R. Eichler, M. A. Garcia, J. M. Gates, S. L. Nelson, R. Sudowe, K. E. Gregorich, D. C. Hoffman, and H. Nitsche, Phys. Rev. C **79**, 027602 (2009).
[21] S. L. Nelson, C. M. Folden III, K. E. Gregorich, I. Dragojević, C. E. Düllmann, R. Eichler, M. A. Garcia, J. M. Gates, R. Sudowe, and H. Nitsche, Phys. Rev. C **78**, 024606 (2008).
[22] G. Münzenberg, P. Armbruster, S. Hofmann, F. P. Heßberger, H. Folger, J. Keller, V. Ninov, K. Poppensieker, A. Quint, W. Reisdorf *et al.*, Z. Phys. A: Hadrons Nucl. **333**, 163 (1989).
[23] S. L. Nelson, K. E. Gregorich, I. Dragojević, M. A. Garcia, J. M. Gates, R. Sudowe, and H. Nitsche, Phys. Rev. Lett. **100**, 022501 (2008).
[24] C. M. Folden III, S. L. Nelson, C. E. Düllmann, J. M. Schwantes, R. Sudowe, P. M. Zielinski, K. E. Gregorich, H. Nitsche, and D. C. Hoffman, Phys. Rev. C **73**, 014611 (2006).
[25] I. Dragojević, K. E. Gregorich, C. E. Düllmann, J. Dvorak, P. A. Ellison, J. M. Gates, S. L. Nelson, L. Stavsetra, and H. Nitsche, Phys. Rev. C **79**, 011602(R) (2009).
[26] S. Hofmann, F. Hessberger, V. Ninov, P. Armbruster, G. Munzenberg, C. Stodel, A. Popeko, A. Yeremin, S. Saro, and M. Leino, Z. Phys. A: Hadrons Nucl. **358**, 377 (1997).
[27] S. L. Nelson, K. E. Gregorich, I. Dragojević, J. Dvořák, P. A. Ellison, M. A. Garcia, J. M. Gates, L. Stavsetra, M. N. Ali, and H. Nitsche, Phys. Rev. C **79**, 027605 (2009).
[28] T. N. Ginter, K. E. Gregorich, W. Loveland, D. M. Lee, U. W. Kirbach, R. Sudowe, C. M. Folden, J. B. Patin, N. Seward, P. A. Wilk, P. M. Zielinski, K. Aleklett, R. Eichler, H. Nitsche, and D. C. Hoffman, Phys. Rev. C **67**, 064609 (2003).
[29] C. M. Folden, K. E. Gregorich, C. E. Düllmann, H. Mahmud, G. K. Pang, J. M. Schwantes, R. Sudowe, P. M. Zielinski, H. Nitsche, and D. C. Hoffman, Phys. Rev. Lett. **93**, 212702 (2004).
[30] K. Morita, K. Morimoto, D. Kaji, H. Haba, E. Ideguchi, R. Kanungo, K. Katori, H. Koura, H. Kudo, T. Ohnishi *et al.*, Eur. Phys. J. A **21**, 257 (2004).
[31] K. Morita, K. Morimoto, D. Kaji, S. Goto, H. Haba, E. Ideguchi, R. Kanungo, K. Katori, H. Koura, H. Kudo *et al.*, Nucl. Phys. A **734**, 101 (2004).
[32] S. Hofmann, F. Hessberger, D. Ackermann, S. Antalic, P. Cagarda, S. Cwiok, B. Kindler, J. Kojouharova, B. Lommel, R. Mann *et al.*, Eur. Phys. J. A **10**, 5 (2001).
[33] K. Morita, K. Morimoto, D. Kaji, H. Haba, E. Ideguchi, J. C. Peter, R. Kanungo, K. Katori, H. Koura, H. Kudo *et al.*, J. Phys. Soc. Jpn. **73**, 1738 (2004).
[34] K. Morita, K. Morimoto, D. Kaji, T. Akiyama, S.-i. Goto, H. Haba, E. Ideguchi, K. Katori, H. Koura, H. Kudo *et al.*, J. Phys. Soc. Jpn. **76**, 043201 (2007).
[35] K. Morita, K. Morimoto, D. Kaji, T. Akiyama, S.-i. Goto, H. Haba, E. Ideguchi, R. Kanungo, K. Katori, H. Koura *et al.*, J. Phys. Soc. Jpn. **73**, 2593 (2004).
[36] K. Morita, K. Morimoto, D. Kaji, H. Haba, K. Ozeki, Y. Kudou, T. Sumita, Y. Wakabayashi, A. r. Yoneda, K. Tanaka *et al.*, J. Phys. Soc. Jpn. **81**, 103201 (2012).
[37] R. Bock, Y. Chu, M. Dakowski, A. Gobbi, E. Grosse, A. Olmi, H. Sann, D. Schwalm, U. Lynen, W. Müller *et al.*, Nucl. Phys. A **388**, 334 (1982).
[38] E. Prokhorova, A. Bogachev, M. Itkis, I. Itkis, G. Knyazheva, N. Kondratiev, E. Kozulin, L. Krupa, Y. Oganessian, I. Pokrovsky *et al.*, Nucl. Phys. A **802**, 45 (2008).
[39] A. J. Pacheco, J. O. Fernández Niello, D. E. DiGregorio, M. di Tada, J. E. Testoni, Y. Chan, E. Chávez, S. Gazes, E. Plagnol, and R. G. Stokstad, Phys. Rev. C **45**, 2861 (1992).
[40] H.-G. Clerc, J. Keller, C.-C. Sahm, K.-H. Schmidt, H. Schulte, and D. Vermeulen, Nucl. Phys. A **419**, 571 (1984).
[41] R. S. Naik, W. Loveland, P. H. Sprunger, A. M. Vinodkumar, D. Peterson, C. L. Jiang, S. Zhu, X. Tang, E. F. Moore, and P. Chowdhury, Phys. Rev. C **76**, 054604 (2007).
[42] K. Hagino, N. Rowley, and A. Kruppa, Comput. Phys. Commun. **123**, 143 (1999).